Supporting Information

Commane et al. 10.1073/pnas.1504131112

Technical Details

Instrument Description. A TILDAS (Aerodyne Research Inc.) was used to measure atmospheric mixing ratios and derive gradients and fluxes of carbonyl sulfide and water vapor at 2,048.495 cm^{-1} and 2,048.649 cm^{-1}, respectively. There were no CO_2 absorption lines in the spectral range of this laser. Mixing ratios of OCS and H_2O at a frequency of 4 Hz (eddy flux) or 1 Hz (gradient flux) were calculated using TDL Wintel software (Aerodyne Research Inc.). A background spectrum (30-s duration) was obtained every 10 min and interpolated and subtracted from the sample spectra to account for any temporal changes in instrument response. A diaphragm pump was used for gradient flux measurements, which resulted in a flow rate of ∼3 standard liters per minute (slm) and cell response time of 15 s (90% response time). The first 60 s at each level were discarded to allow for equilibration of water vapor. The 1σ instrumental precision was 5 pptv ($pmol{\cdot}mol^{-1}$) in 1-s averaging down to 0.9 pptv at 100 s. During eddy flux measurements, a TriScroll 600-slm pump resulted in a flow rate of 12 slm through the cell and a response time of 1 s. The 1σ instrument precision was typically 14 pptv at 4 Hz, likewise averaging down to <1 pptv at 60 s. The sensor is a further development of previous work (17, 18).

The combined water vapor dilution and pressure broadening correction factor was 1.27 at this wavelength, which, if not corrected, could have caused an underestimation of 7 pptv (in 400 pptv) OCS for 14 ppth ($mmol{\cdot}mol^{-1}$) water vapor. This correction has been applied to the dataset. A NOAA-calibrated cylinder of OCS in air was regularly added to the gradient flux setup (flow rate ∼3 slm); however, the high flow rate of the eddy flux method (∼12 slm from August 4) made frequent overblowing of the inlet with a constant flow difficult and expensive. Instead, the regular additions of OCS-free air for the null spectra were used to determine the temporal variations in the instrument stability, with less frequent addition of the calibration gas. These calibrations were independent of the NOAA flask samples described below.

Fig. S1 shows a time series of OCS measured by the TILDAS (30-min average) and OCS measured in weekly/fortnightly paired flask samples analyzed by gas chromatography with mass spectrometric detection at NOAA [update of measurements from Montzka et al. (1)]. Most flask samples were collected at midday over a few minutes, after extensive flushing. The TILDAS measurements show short-term variability, often greatest outside of midday, that cannot be observed by the flasks. However, when the TILDAS data are averaged for the time periods around the flask sampling time (gray circles in Fig. S1), both measurements track well.

Calculation of OCS Fluxes. Two methods were used to calculate the canopy scale flux of OCS (F_{OCS}) at Harvard Forest. The gradient flux method was used between January 2011 and early August 2011, followed by the eddy covariance method, which continued until the end of the year.

Gradient flux method. The micrometeorological gradient flux method, also known as the modified Bowen ratio method (46), is based on the assumption of trace gas similarity between OCS and, in our measurements, H_2O to calculate the flux of OCS, gF_{OCS} ($pmol{\cdot}m^{-2}{\cdot}s^{-1}$):

$$gF_{OCS} = F_{H_2O}\ gOCS/gH_2O, \qquad \text{[S1]}$$

where gOCS ($pmol{\cdot}mol^{-1}{\cdot}m^{-1}$) and gH_2O ($mmol{\cdot}mol^{-1}{\cdot}m^{-1}$) are the vertical concentration gradients of OCS and H_2O, respectively, measured simultaneously by the TILDAS at two heights (29.5 m and 24.1 m),

$$gX = [X]_{29.5m} - [X]_{24.1m}/(29.5 - 24.1), \qquad \text{[S2]}$$

and the water vapor flux F_{H2O} is measured directly by eddy covariance at the EMS tower using a infrared gas analyzer [IRGA; Li-COR 6262 (24)]. The nominal TILDAS water vapor mixing ratios were 22% higher than the calibrated water vapor mixing ratios measured by the IRGA. The water vapor observed by the TILDAS was based on spectroscopic parameters and was not externally calibrated, so this correction was applied to the TILDAS water vapor mixing ratios before calculation of the gradient flux.

The OCS flux could not be calculated for 23% of the OCS measurements made during the May–August 2011 sampling period. This was due to a combination of rain events (when no water vapor flux was calculated) and unrealistic water vapor mixing ratios (ΔH_2O outside the 95% quantiles of the total data), which resulted in equally unrealistic OCS fluxes. Fig. S4 shows the diel cycle of the measurements of OCS gradient (Fig. S4*A*) and H_2O gradient (Fig. S4*B*), the H_2O flux measured by eddy flux (Fig. S4*C*), and the calculated OCS flux using the gradient flux method (Fig. S4*D*) for June 14, 2011. The CO_2 flux measured by eddy covariance (Fig. S4*E*) is included for comparison. Negative fluxes indicate loss from the atmosphere and uptake by the biosphere.

The overall uncertainty of the gradient flux method was calculated for each point as the root-mean-square of the 95% confidence intervals of the gradient measurements (gOCS and gH_2O) and the mean error of the eddy covariance calculated water vapor [15% (24)]. As the instrument is optimized to OCS detection, the error in the water vapor gradient measurement, combined with the SD of the water vapor mixing ratio within a 30-min period, dominated the overall uncertainty. For the June–July period, the uncertainty in absolute fluxes ranged from 0.05 $pmol{\cdot}m^{-2}{\cdot}s^{-1}$ to 20 $pmol{\cdot}m^{-2}{\cdot}s^{-1}$ on rare occasions with a median of 0.43 $pmol{\cdot}m^{-2}{\cdot}s^{-1}$. For example, as shown in Fig. S4, this uncertainty reaches a maximum of 5.7 $pmol{\cdot}m^{-2}{\cdot}s^{-1}$ for an OCS flux of 1.1 $pmol{\cdot}m^{-2}{\cdot}s^{-1}$ on June 14, 2011.

For the gradient flux method, ambient air was alternatively sampled from the tower heights of 29.5 m and 24.1 m using 40 m of 3/8" (OD; 0.95 cm) Synflex tubing. Teflon particle filters (pore size 5 μm) at the inlet of each sampling line were changed every 2–4 wk to prevent artificial production of OCS on chemically aged or dirty surfaces (*Artificial OCS Production*). These filters resulted in a pressure drop through the tubing, which reduced the effects of adsorption/desorption on the tubing. The black Synflex tubing also reduced any sunlight effects on the sample. The air in each sampling tube was tested after each background (10- or 30-min interval) to ensure no in situ production of OCS (short-lived increase in OCS). The materials in the instrument were carefully chosen to minimize any artifacts during sampling: clean Teflon filters, Synflex tubing, stainless steel solenoid valves, and the glass sampling cell were not found to scavenge or emit OCS. No pump was used upstream of sampling to prevent contamination of the sample gas. Some initial measurements were made at 25 m and 1 m during the winter of 2010–2011. The calculated fluxes for this winter 2011 period agreed with eddy fluxes for winter 2012, so these early data have been included in the seasonal cycle of F_{OCS}. For eddy covariance flux measurements, only the 29.5-m inlet was used.

The gradient flux method has been used successfully at Harvard Forest previously to measure fluxes of hydrogen (47), nonmethane hydrocarbons (48, 49), and isoprene (50). In each of these studies, the use of CO_2, H_2O, and air temperature produced similar fluxes throughout the year with varying precision and accuracy. These methods were further validated by McKinney et al. (51), who found very similar fluxes of isoprene using a disjunct eddy covariance method, compared with Goldstein's gradient flux method. Particularly relevant to the study here, Meredith et al. (47) found that the gradient flux method using either H_2O or CO_2 was valid throughout 2011.

To test scalar similarity using water vapor during the anomalous hot period in July, we calculated the OCS flux using the CO_2 gradient and flux from the eddy covariance system (Fig. S5). The CO_2 gradients are smaller than H_2O, and the top levels are measured less frequently, which introduces additional noise to the calculated flux compared with the flux calculated from H_2O. The OCS flux calculated based on CO_2 shows the same seasonal cycle for both day and night data as OCS from water vapor but with substantially more noise in the CO_2-based flux, as expected. Fig. S5 shows F_{OCS} for the July 21–31 OCS emission period calculated from H_2O ($FOCS_{H2O}$) and CO_2 ($FOCS_{CO2}$). Regardless of the method used, statistically significant emission of OCS was observed throughout the day in the July period.

Eddy covariance method. The eddy covariance fluxes of OCS (eF_{OCS}) and H_2O (eF_{H2O}) were calculated from high-frequency (4 Hz) measurements of OCS and H_2O made by the TILDAS at 29.5 m. After subtracting a block average for the interval, the covariance of the residual of the vertical wind velocity (w′) and concentration (OCS′ or H_2O') for each 30-min interval was calculated as in Goulden et al. (21), e.g.,

$$F_{OCS} = \overline{w'OCS'} \quad eF_{OCS} = w'\mathrm{OCS} \quad eF_{H_2O} = w'\mathrm{H_2O'}. \qquad \textbf{[S3]}$$

The instrument synchronization time lag was determined by maximizing the correlation between w′ and H_2O'. This lag also accounted for differences in computer clock times between the sonic and OCS data systems, which increased gradually after each synchronization reset (daily). The flux is rotated to the plane where the mean vertical wind is zero (52). The calibrated IRGA water vapor fluxes were used for all analysis. Accurate fluxes can be calculated even though high-frequency noise limits the precision of the OCS concentration at short times because the noise is not correlated with vertical wind velocity. The error in the eddy covariance was determined by calculating the root-mean-square combination of observed covariance for periods ±25 s from the lag time. This resulted in a mean SE in the eddy covariance calculated OCS flux of 14%.

Gradient flux and eddy covariance comparison. Both gradient measurements and eddy flux measurements were made for a limited time period, 6–12 August 2011, when additional measurements were made at a height of 24.1 m for 120 s every 30 min. This shorter sampling period at 24.1 m resulted in a greater error in the gradient flux (gF_{OCS}) for this period (47). In a comparison of the two methods, the composite diel cycle (2 hourly bins) of gF_{OCS} (Fig. S6, black circles) and eF_{OCS} (Fig. S6, red boxes) for periods of common measurements showed similar behavior but with slightly more variance in gF_{OCS}, as expected. The overall trend through the composite day compares well for both methods, with no statistical difference between the daily mean flux calculated by either method: daily mean OCS uptake of −8.6 (± 6.2; 95% CI) pmol·m^{-2}·s^{-1} for gF_{OCS} and −9.6 (± 4.4) pmol·m^{-2}·s^{-1} for eF_{OCS}. The gradient flux of OCS underestimates the total daily flux (gF_{OCS} = −174 pmol·m^{-2}·s^{-1}) by 7% compared with the eddy flux (eF_{OCS} = −187 pmol·m^{-2}·s^{-1}). The signs and the diel patterns of the flux are consistent for both methods, except during transition periods near sunrise and sunset when fluxes, especially the water vapor flux used to calculate gF_{OCS}, are small and neither method is reliable.

OCS storage. The actual net uptake or emission of a trace gas by the ecosystem is the observed vertical flux plus any accumulation (or depletion) in the canopy space below the flux sensor (storage term). For CO_2, the storage term is significant compared with the vertical flux, especially around dawn and dusk transitions, disregarding nonideal conditions with significant horizontal advective fluxes. Although the storage term sums to nearly 0 over a daily interval, it must be included to interpret net CO_2 exchange on subdaily intervals. During summer 2012 (and when large CO_2 storage values were calculated), changes in storage of OCS calculated from OCS profile measurements were negligible. The physical processes affecting storage should not change from year to year, so the contribution to the ecosystem flux of OCS from 2012 should be applicable to 2011. Therefore, storage has been neglected in the OCS flux results that we report here.

Artificial OCS Production. Heterogeneous production of OCS on the surface of the contaminated Teflon filters was observed over 5 d after sampling an anthropogenically influenced air mass in February 2011 because unsafe climbing conditions prevented immediate replacement of the filter, which had been in place since late December. This OCS production was observed as large, short-lived pulses of OCS (up to 800 pptv) when sampling the line (and contaminated filter) after zero air background measurements. However, no evidence of OCS production from filter contamination was observed during the summer emission period described in the main text. Air mass trajectories for this February event indicate that the air was influenced by high sulfur emission from the copper and nickel smelters in Sudbury, ON, Canada, and SO_2 mixing ratios of greater than 60 ppbv were observed in the same air mass at a site 60 miles east of Harvard Forest (Aerodyne Research) on the same day. OCS dissolves, but is not hydrolyzed, in acidic water. Belviso et al. (53) measured supersaturated OCS in acidic rainwaters in France and suggested an in situ production of OCS from the acid catalyzed reaction of thiocyanate salts. No further studies have confirmed this suggested mechanism. However, the emission of high mixing ratios of OCS from Teflon filters could be related to a similar production mechanism because OCS production continued for a number of days and was increased in warmer, and slightly more humid, daylight conditions. There is limited literature on the heterogeneous production of OCS and potential mechanisms should be investigated in future studies. Data with contaminated filter production of OCS have been removed from further analysis and from Fig. S1.

Materials for the instrumental setup were carefully chosen to ensure no artificial production of OCS in the system. Testing showed that OCS was produced by rubber diaphragms in pumps and resulted in strong OCS production (pulses up to 24 ppb) in recirculating soil chambers at Harvard Forest. No soil chamber data were used in the analysis presented here. Neoprene and plastic tubing, which are often used in soil chambers, were particularly strong producers of OCS. Clean Synflex and Teflon tubing were not found to produce observable OCS. Although steps have been taken to minimize the effect of material contamination and to remove any data influences by atmospheric contamination, it is possible that the large OCS emission observed in July may be the result of some unknown physical production mechanism. In their studies of OCS in a wheat field, Maseyk et al. (8) observed OCS emission of 217 μg S per m^2 over the final 10 d of measurements (from a total of 657 μg S per m^2 over 7 wk). We estimate a comparable OCS emission of 207 μg S per m^2 over the 10 d of observed net OCS emission at Harvard Forest.

Soil warming and nitrogen fertilization experiments have been conducted in plots to the SW of the tower from 2006 to present, including during 2011 (54). These experiments use ammonium nitrate (NH_4NO_3) to fertilize 12 plots of size 3 × 3 m. The fertilizer

contains trace levels of sulfur (~0.002% sulfur as SO_4^-), which is equivalent to an application of 2.2 g S per ha per y, a less than 0.01% increase on the sulfur content of the soil. The periods of OCS emissions were not found to correlate with the application of the fertilizer. Although we cannot discount the possibility of an OCS artifact from the fertilizer, we suspect that the small area involved and the low levels of sulfur application are too small to contribute to the observed OCS signal. Nitrogen fertilization experiments also found increased OCS emission from soils (55), but we do not see a correlation with soil temperature and the related increase in microbial activity. It is possible that the sulfur present in the soils at Harvard Forest, like the soils of the wheat fields in Oklahoma (8), is a source of OCS through some unknown biophysical mechanism.

Site Description and Ancillary Measurements

Site Description. Measurements were made at the Environmental Measurement Site (EMS) at Harvard Forest, Petersham, MA (42.54°N, 72.17°W, elevation 340 m). The CO_2 flux into and out of the forest has been measured at this LTER site since 1990 (24). The 30-m meteorology tower extends about 5 m over the forest canopy and is located on moderately hilly terrain surrounded by several kilometers of relatively undisturbed forest; ~80% of the turbulent fluxes are produced within 0.7–1 km of the tower (56). The basal area ($m^2 \cdot ha^{-1}$) of various tree species within the footprint of the tower is tracked on plots established in 1993. In 2011, the southwest sector was dominated by deciduous species red oak (20.0% basal area) and red maple (11.8%) with some black oak (2.6%) and ash (2.1%). The northwest sector was more mixed with red oak (17.3%) and hemlock (13.2%) dominating and some red maple (9%), red pine (7.3%), and white pine (5.4%). A dried up pond, which is now an area of new tree growth, was also located in the northwest sector.

Soils at Harvard Forest are acidic and originate from sandy loam glacial till. The diversity and richness of the soil microbial community is somewhat reduced at low soil pH (57), but the soil at Harvard Forest contains representatives of the phyla typical in most soils, many of which can encode for one or more carbonic anhydrase enzymes (29).

CO_2 Flux Measurements. The CO_2 flux at the EMS tower was measured by eddy covariance as described extensively in previous work (21, 24) and in Figs. S5–S7. The CO_2 flux term accounts for storage of CO_2 within the canopy as determined from gradient measurements of the CO_2 concentration (58). The daytime respiration of CO_2 is projected from the observed temperature dependence of respiration at night. To estimate gross ecosystem productivity (GEP) from the measured CO_2 flux, we use the difference between the daytime CO_2 flux and the projected daytime respiration (21).

The Hemlock Tower is another flux tower at Harvard Forest located 500 m away from the EMS tower in a mature hemlock stand. The CO_2 uptake by conifer species in 2011 was found to be greatest in April, May, and June (2.1–2.4 g C per m^2 per d) before being drastically reduced in July (0.5 g C per m^2 per d), recovering in August (1.5 g C per m^2 per d) and reducing in the fall (0.4–0.6 g C per m^2 per d; September–October). The conifer uptake flux increased again in November (1.1 g C per m^2 per d) with higher air temperatures before essentially stopping in December (0.008 g C per m^2 per d).

Sap Flow Measurements. Ecosystem-scale flux observations cannot distinguish the canopy flux from the soil flux, because both sinks are located beneath the flux measurement point. Measurements of sap flow through trees (i.e., water uptake by trees) provide understanding of whole-tree transpiration with high temporal resolution when measured continuously throughout the growing season. Because both transpiration and photosynthesis are controlled by stomatal conductance, measurements of sap flow and eddy flux can be combined to understand patterns of canopy carbon uptake (59). We measured rates of sap flow (60) in the dominant (by mass) deciduous tree species [*Quercus rubra* (northern red oak) and *Acer rubrum* (red maple)] in a nearby site at Harvard Forest during a period that overlapped with OCS flux measurements (Figs. S3 and S7). These measurements provide an indication of tree activity that has been used to understand the observed OCS (and CO_2) fluxes. Two sensors were installed at breast height on six individual red oak red maple trees (24 sensors total).

Sap flow rates in both species began to increase on May 19, just after bud break. Senescence began around late October, with water uptake by the red oak continuing until about November 13. Elevated sap flow was generally observed before midnight throughout the growing season before reducing to minimal levels in the early hours of the morning. Fig. S7 shows the summer sap flow rates staying high into the late afternoon after both PAR and the water vapor flux began to decrease. The bulk tree activity, as observed by sap flow rates, showed that the red oaks continued to be active for up to 5 h into the night before reaching zero.

OCS:CO_2 Atmospheric and Ecosystem Relative Uptake

The effect of vegetative uptake on ambient OCS mixing ratios can be explored by looking at a ratio of OCS to CO_2. The atmospheric relative uptake (ARU) is the seasonal change in the OCS:CO_2 uptake ratio (1):

$$\mathrm{ARU} = \frac{[\mathrm{OCS}]_{\mathrm{max-min}}}{[\mathrm{OCS}]_{\mathrm{annual\_mean}}} \times \frac{[\mathrm{CO_2}]_{\mathrm{annual\_mean}}}{[\mathrm{CO_2}]_{\mathrm{max-min}}}, \qquad \mathbf{S4}$$

where $[X]_{\mathrm{max\text{-}min}}$ is the difference between spring maximum and autumn minimum ambient mixing ratios of OCS and CO_2 normalized by their annual mean. We calculate an ARU of 8.5 for 2011, which is similar to the ARU (~8 ± 2) calculated from a multiannual analysis of flask data collected at Harvard Forest for 2000–2005 (1).

The ratio of the ecosystem flux per molecule of OCS to the flux per molecule of CO_2 (f_{OCS}:f_{CO2}) can also be compared with the ecosystem relative uptake (ERU) of OCS to CO_2, reported for studies on larger scales (1, 13). The ERU calculated from aircraft profile data [4.6–6.5 for the New England area in July–August 2004 (13)], was higher than the f_{OCS}:f_{CO2} ratio calculated for the Harvard Forest flux tower in this study: during summer months when photosynthesis was greatest (June–September, excluding July), the mean daily f_{OCS}:f_{CO2} ratio was 2.6 ± 0.7, and the mean daytime (PAR > 300 $\mu E \cdot m^{-2} \cdot s^{-1}$) f_{OCS}:f_{CO2} ratio was 1.5 ± 0.3. The f_{OCS}:f_{CO2} ratio increased from August through October (Table S1). This difference between the aircraft (regional scale) and the tower (local scale) is likely due to the larger nonvegetative sources of CO_2 (including anthropogenic) than OCS (marine and anthropogenic) in the wider region not present within the tower footprint. This example illustrates the value of F_{OCS} data for interpretation of large scale CO_2 signals.

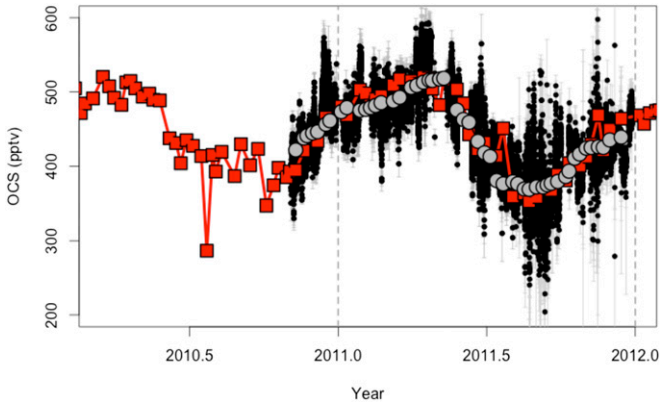

Fig. S1. Comparison of OCS (pptv; pmol·mol^{-1}) measured by the TILDAS [30-min average (black) with 1σ SDs shown in gray], NOAA flask pair means [red points; 1σ SDs shown as red line error bars (barely visible)], and cosampled TILDAS OCS [3-h average at the time of the flask sample (gray circles)]. The flasks were sampled weekly followed by analysis by GC-MS in Boulder as part of the NOAA flask sample network (1).

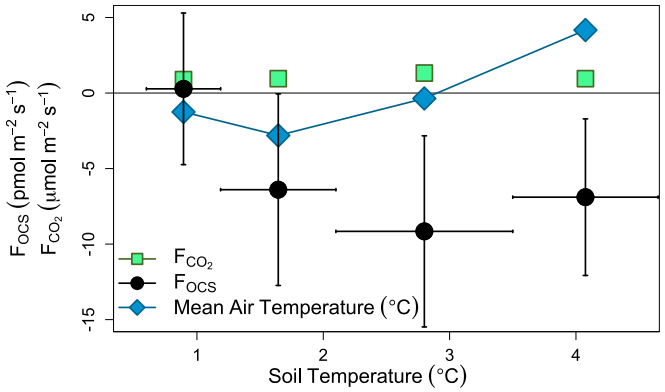

Fig. S2. The OCS (black circles; pmol·m^{-2}·s^{-1}) flux, CO_2 flux (green squares; μmol·m^{-2}·s^{-1}), and the air temperature (blue diamonds; °C) for given surface soil temperatures in December 2011. The data are partitioned to have equal numbers of data points for each temperature shown.

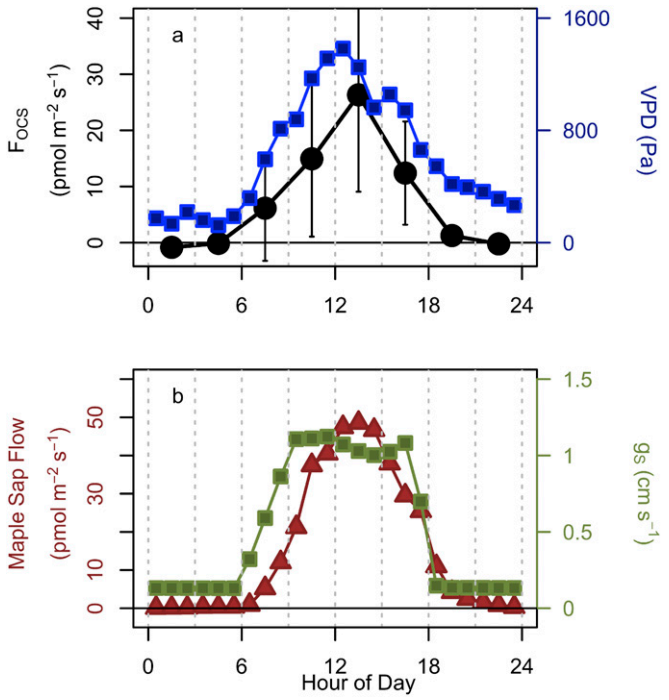

Fig. S3. Diel cycles of (*A*) F_{OCS} (black circles; pmol·m^{-2}·s^{-1}) and VPD (blue squares; Pa) and (*B*) bulk sap flow rate for maple trees (brown triangles; gH_2O·m^{-2}·s^{-1}) and stomatal conductance (g_S; green squares; cm·s^{-1}) for the anomalous OCS emission period on July 19–31, 2011.

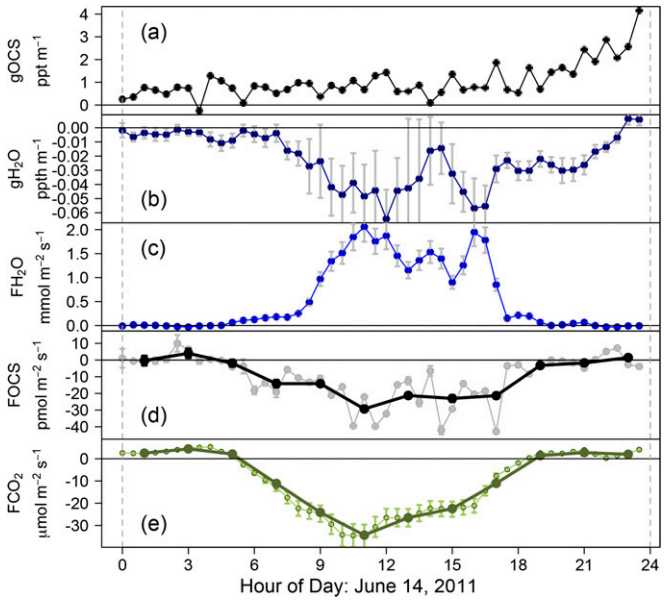

Fig. S4. Components of gradient flux calculated OCS flux for June 14, 2011. (*A*) gOCS: OCS gradient (black; pptv·m^{-1}), confidence intervals of the OCS gradient (gray bars, which are barely visible). (*B*) gH_2O: H_2O gradient (dark blue; pptv·m^{-1}), confidence intervals of H_2O gradient (gray bars). (*C*) FH_2O: H_2O flux (blue; mmol·m^{-2}·s^{-1}), 15% error on eddy covariance measurements (gray bars). (*D*) gFOCS: OCS gradient flux (pmol·m^{-2}·s^{-1}), 2-h average (black), and 30-min gFOCS (gray points with SE as gray bars). (*E*) FCO_2: CO_2 flux (as NEE including storage contribution) (µmol·m^{-2}·s^{-1}), 30-min FCO_2 (small light green points), 15% error on eddy covariance measurements (green bars), 2-h mean (dark green points).

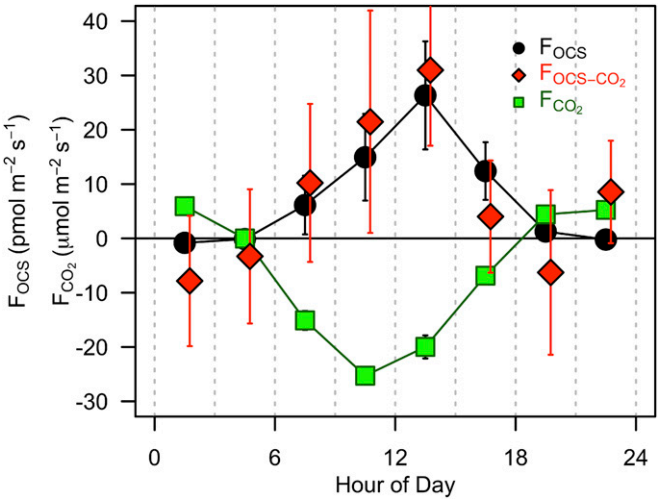

Fig. S5. Composite diel cycle of the gradient flux OCS derived from gradients of water vapor ($F_{OCS.H2O}$; black points) and carbon dioxide ($F_{OCS.CO2}$; red squares) for coincident data in 3 hourly time bins for July 19–31, 2011. The error bars indicate the 95% confidence intervals of the data within the composite 3-h period.

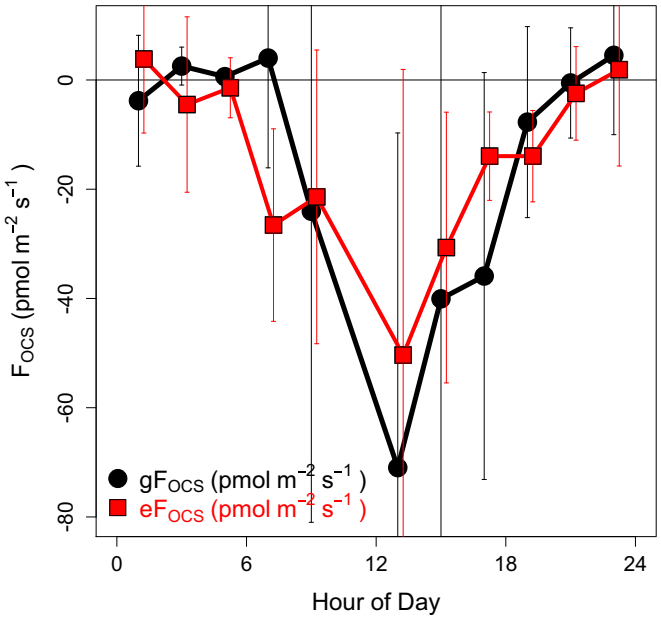

Fig. S6. Composite diel cycle of the gradient flux OCS (gF_{OCS}; black points) and eddy covariance OCS flux (eF_{OCS}; red squares) for coincident data in 2 hourly time bins for August 6–12, 2011. The error bars indicate the 95% confidence intervals of the data within the composite 2-h period.

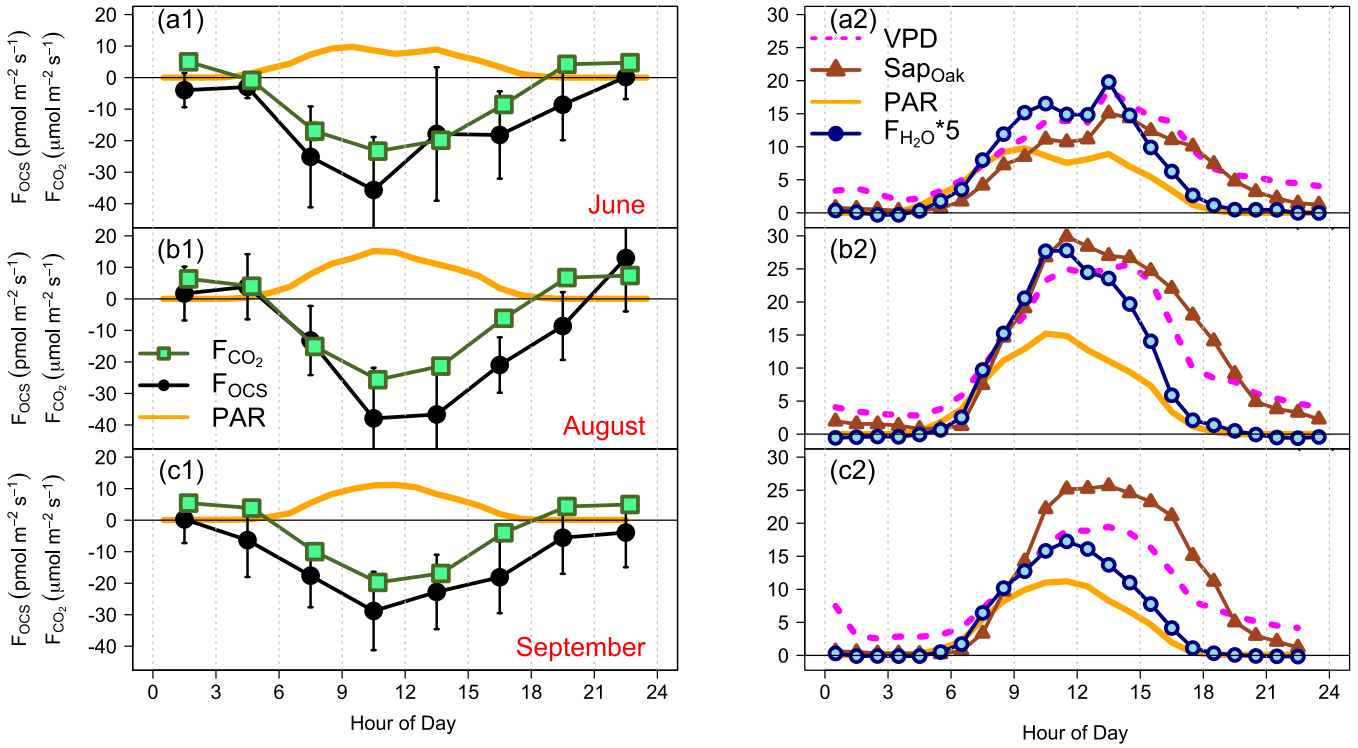

Fig. S7. Diurnal composite of OCS (black) and CO_2 (green) fluxes (Eastern Standard Time) for the summer months of 2011: (*A1*) June, (*B1*) August, and (*C1*) September, with times of low turbulence ($u^* < 0.17$ m·s^{-1}) removed. The 95% confidence intervals for each species are shown as black error bars. The 95% confidence intervals for CO_2 are barely visible. Both columns show PAR (solid orange line; 10^{-8} E·m^{-2}·s^{-1}) on two different scales. *A2*, *B2*, and *C2* show the sap flow rates for oak (brown triangles; gH_2O·m^{-2}·s^{-1}), the vapor pressure deficit (magenta dashed line; Pa), and the water vapor flux [blue/navy circles; 5 mmol·m^{-2}·s^{-1} (multiplied by 5 for graphing)] for June, August, and September.

Table S1. Monthly mean normalized flux

Normalized flux	April	May	June	July	August	September	October	November	December	Year mean
f_{OCS}, m s^{-1}	−0.4	−0.7	−1.3	0.7	−1.6	−1.7	−0.8	−0.5	−0.4	−0.9
f_{OCS}, mmol m^{-2} s^{-1}	−9	−17	−31	18	−39	−43	−18	−10	−10	−22
f_{OCS}/f_{CO2} (ERU)		−0.4	0.7	−2.0	0.8	2.4	3.7	−9.6	5.2	1.4*
f_{OCS}/f_{GEP} (LRU)		1.5	0.5	−0.4	1.2	1.2	0.7	6.6	9.4	1.0*

Monthly mean of ecosystem flux per molecule of OCS (f_{OCS}, m·s^{-1}); ecosystem flux per mole of OCS (f_{OCS}, mmol·m^{-2}·s^{-1}); ratio of the flux per molecule of OCS to that of CO_2 (f_{OCS}/f_{CO2}), comparable to the ERU; and ratio of the flux per molecule of OCS to that of GEP (f_{OCS}/f_{GEP}), comparable to the LRU for daylight hours (PAR > 300 μE·m^{-2}·s^{-1}). Note: Period of net OCS emission in July. This has been removed from the mean year calculation.

*Only the growing season mean (June–October 2011, excluding July) was calculated for f_{OCS}/f_{CO2} and f_{OCS}/f_{GEP} instead of an annual mean. Only data with $u^* > 0.17$ m·s^{-1} have been used in the calculations.